Fast-ion Dα measurements of the fast-ion distribution (invited)[a)]

W. W. Heidbrink[b)]
University of California, Irvine, California 92697, USA

(Presented 18 May 2010; received 13 May 2010; accepted 23 June 2010; published online 25 October 2010)

The fast-ion Dα (FIDA) diagnostic is an application of charge-exchange recombination spectroscopy. Fast ions that neutralize in an injected neutral beam emit Balmer-α light with a large Doppler shift. The spectral shift is exploited to distinguish the FIDA emission from other bright sources of Dα light. Background subtraction is the main technical challenge. A spectroscopic diagnostic typically achieves temporal, energy, and transverse spatial resolution of ~1 ms, ~10 keV, and ~2 cm, respectively. Installations that use narrow-band filters achieve high spatial and temporal resolution at the expense of spectral information. For high temporal resolution, the bandpass-filtered light goes directly to a photomultiplier, allowing detection of ~50 kHz oscillations in FIDA signal. For two-dimensional spatial profiles, the bandpass-filtered light goes to a charge-coupled device camera; detailed images of fast-ion redistribution at instabilities are obtained. Qualitative and quantitative models relate the measured FIDA signals to the fast-ion distribution function. The first quantitative comparisons between theory and experiment found excellent agreement in beam-heated magnetohydrodynamics (MHD)-quiescent plasmas. FIDA diagnostics are now in operation at magnetic-fusion facilities worldwide. They are used to study fast-ion acceleration by ion cyclotron heating, to detect fast-ion transport by MHD modes and microturbulence, and to study fast-ion driven instabilities. © *2010 American Institute of Physics.* [doi:10.1063/1.3478739]

I. INTRODUCTION

Hydrogenic superthermal energetic ions are present in most magnetic fusion experiments. These fast ions are injected by neutral beams or accelerated by wave heating. Many aspects of plasma behavior cannot be understood without knowledge of the fast-ion distribution function.

In recent years, a new technique has emerged as a powerful diagnostic of the fast-ion distribution function. This technique, known as fast-ion Dα (FIDA), exploits visible light emitted by energetic deuterium ions as they pass through a neutral beam. Similar measurements of energetic helium ions were made in the 1990s.[1,2] The first FIDA measurements were made on the DIII-D tokamak and published in 2004.[3] In 2007, FIDA diagnostics were installed on the National Spherical Torus Experiment (NSTX).[4] By now, FIDA diagnostics are installed or are under development at six magnetic fusion facilities. The purpose of this paper is to summarize FIDA research in its initial stage of development.

Section II discusses the measurement itself: the underlying atomic processes, the challenge of distinguishing the FIDA light from other bright sources in the spectral range of interest, and the instrumentation employed to date. Section III considers the relationship between the measured light and the desired quantity, the fast-ion distribution function. The final section (Sec. IV) summarizes past, present, and future applications of the diagnostic.

II. THE FIDA MEASUREMENT

A FIDA measurement is an application of charge-exchange recombination spectroscopy.[5] The basic process is illustrated in Fig. 1(a). A deuterium ion orbits through a neutral beam and a charge exchange event occurs, neutralizing the fast ion. Since it is uncharged, the neutralized fast ion travels in a straight line. Often the fast neutral is in an excited atomic state. As it travels, it may change its energy level either through collisions with the plasma or through radiative decay. If it undergoes a Balmer-α transition, which is a transition from the $n=3$ to the $n=2$ level, it emits a visible Dα photon.

Figures 1(b)–1(d) describe the process in more detail. The probability of the initial neutralization event depends strongly on the relative velocity between the fast ion and the injected neutral. In reality, four neutral populations are important. The injected neutral beam has a full-energy, half-energy, and third-energy component. In addition, charge-exchange events with the bulk thermal deuterium population create a cloud of "halo" neutrals in the vicinity of the injected beam. The density of this halo neutral population is comparable to the injected neutral densities. These four neutral populations each have their own distributions of excited states. Although the occupation of the ground state far exceeds the occupation levels for excited states, the probability that the fast ion will arrive in the $n=3$ state after a charge-

[a)]Invited paper, published as part of the Proceedings of the 18th Topical Conference on High-Temperature Plasma Diagnostics, Wildwood, New Jersey, May 2010.

[b)]Electronic mail: bill.heidbrink@uci.edu.

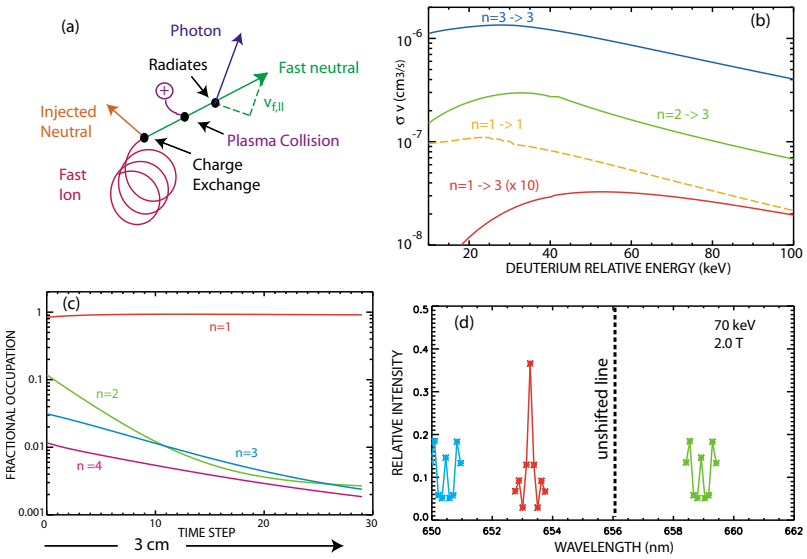

FIG. 1. (Color online) (a) The FIDA process. A fast ion traverses a neutral beam and is neutralized in a charge exchange reaction. The atomic energy levels change while the neutral propagates. Some neutrals radiate a Dα photon that is Doppler shifted by the velocity component in the direction of emission. (b) Charge exchange reactivities for transitions from various energy levels to the $n=3$ level. The abscissa is the relative energy between the ion and neutral computed from the relative velocity. Note that transitions from the ground state are ten times less probable than shown. (c) Time evolution of level occupations obtained from solution of the collisional-radiative transition equations for 80 keV neutrals in a DIII-D discharge. The neutral only travels a few centimeters before the $n=3$ occupation level decays to a negligible level. (d) Sample of spectra from 70 keV neutrals for various velocity vectors relative to the photon and magnetic-field directions. The shift from 656.1 nm (dashed line) is due to the Doppler shift; the line splitting is caused by the motional Stark effect.

exchange reaction with a ground-state neutral is very low; see the reactivity σv for a $n=1\rightarrow3$ reaction in Fig. 1(b). In contrast, the occupation levels for excited states in the injected beam are below 1% but the reactivities for $n=2\rightarrow3$ and $n=3\rightarrow3$ reactions are orders of magnitude larger than for ground-state donors. The result is that reactions from the $n=1$, 2, and 3 levels all make comparable contributions to the number of neutralized fast ions in the $n=3$ state. Consequently, the initial population of neutralized fast ions is far from equilibrium. Figure 1(c) shows a typical example of the subsequent relaxation of the neutral population toward equilibrium values. These curves are calculated by solving the collisional-radiative equations that describe transitions between atomic energy levels. The fast neutral only travels a few centimeters before the $n=3$ population has decayed. Some ($<44\%$) of the $n=3$ neutrals emit a Balmer-α photon. The spectrum of these photons depends on both the Doppler shift and on Stark splitting; Fig. 1(d) shows three examples of the relative importance of these two factors. The unshifted Dα line is at 656.1 nm. The Doppler shift provides information on one component of the initial fast-ion velocity and shifts the line 2–6 nm. The Stark splitting is caused primarily by the motional Stark effect and so depends on the velocity $\vec{v}$ of the neutral relative to the magnetic field $\vec{B}$. The $\lesssim1$ nm (for $B\cong2$ T) Stark splitting effectively acts as a line-broadening mechanism that degrades the spectral resolution of the measurement.

Figure 2 shows a quantitative example of these atomic physics considerations for a typical DIII-D case. Distributions of initial occupation levels are plotted in Fig. 2(a). Because of the strong cross-section effect [Fig. 2(b)], the initial occupation levels of the $n=2-4$ states exceed 1%. These levels are an order of magnitude higher than the equilibrium levels in this region of the plasma, which are of order 0.1%. As a result, rapid adjustment of the energy levels occurs, as illustrated for one case in Fig. 1(c). Figure 2(b) shows the average distance traveled before a photon is emitted for the ensemble of initial states shown in Fig. 2(a). Within 2 cm of the neutralization event, nearly 100% of the Dα photons have been emitted. This is consistent with a rough estimate: A typical fast-ion velocity is 2×10^8 cm/s and the combined $3\rightarrow1$ and $3\rightarrow2$ radiative decay rate is 10^8/s, with collisions increasing the decay rate still further. The rapid decay from highly excited levels has the important implication that the intrinsic spatial resolution of the FIDA technique is <2 cm. (Reference 3 and subsequent publications erroneously state that the intrinsic resolution is ~5 cm.) In conventional charge-exchange recombination spectroscopy with impurity ions, a "plume" effect can degrade the spatial resolution of the measurement[7] but, for FIDA, because the excited atom is neutral, the subsequent trajectory is unaffected by the magnetic field. Although the transverse spatial resolution can be

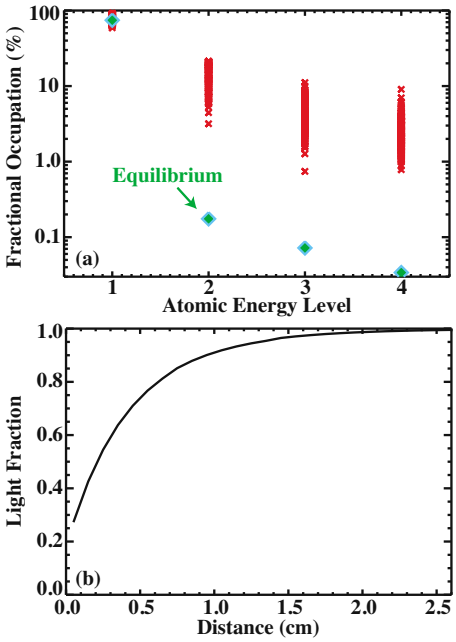

FIG. 2. (Color online) (a) Distribution of initial energy levels (x) for an ensemble of reactions in DIII-D discharge No. 132607 (Ref. 6). The diamond symbols represent the equilibrium distribution of states at the same location in the plasma. (b) Distance traveled by the atom before radiating a Dα photon for the distribution shown in (a). (The calculation includes the charge-exchange reaction probabilities for the various initial conditions.) Nearly all of the light is emitted within a distance of 2 cm.

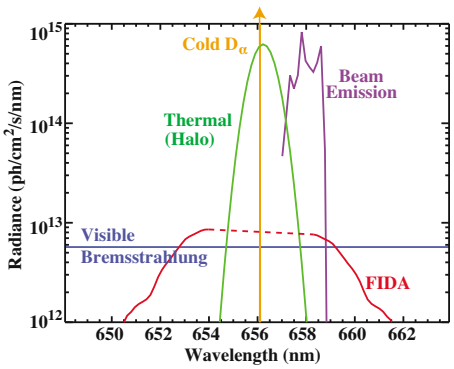

FIG. 3. (Color online) Various sources of light in the Dα spectral band for a typical case. The spectral intensity of Dα light from edge neutrals is largest. Radiation from injected neutrals and from halo neutrals is an order of magnitude larger than the FIDA and visible bremsstrahlung spectral features.

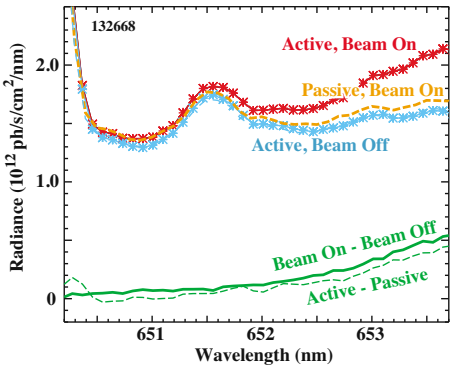

FIG. 4. (Color online) Comparison of different methods of background subtraction for a NSTX discharge with average beam power of only 0.5 MW. The blueshifted side of the spectrum is shown. The two spectra labeled "active, beam on" and "active, beam off" are from a fiber that views the injected neutral beam; the difference of these signals is the FIDA spectrum obtained from beam modulation and is labeled "beam on-beam off." The dashed line labeled "passive, beam on" is from a toroidally separated view acquired when the injected beam is on. (A slight difference in passive signal is observed during beam modulation.) The dashed FIDA spectrum labeled "active-passive" is obtained using this signal to subtract the background. Passive impurity lines at 650.0 and 651.5 nm are evident in the raw spectra but disappear upon background subtraction.

small, the resolution along the line of sight is determined by the extent of the neutral beam and its halo. For example, for a vertical view on DIII-D, the vertical full width at half maximum is ~30 cm.

The principal challenge in a FIDA measurement is distinguishing the FIDA signal from other bright sources of light in the same spectral region. The intensity of the beam emission spectrum (BES) radiated by the injected neutrals is typically two orders of magnitude larger than the FIDA signal (Fig. 3). Dα light from halo neutrals is comparable to the injected neutral light. To make a successful measurement, the viewing geometry must be selected to Doppler shift the FIDA feature away from the BES feature and away from the unshifted Dα line. The original FIDA measurements utilized a vertical view[3] but, in recent years, tangential geometries have been successfully employed (for example, Refs. 6 and 8). Other contaminants in the spectrum include impurity lines, visible bremsstrahlung, and the very bright emission from atomic deuterium at the edge of the device. Impurity lines are usually removed by fitting. Visible bremsstrahlung is removed by background subtraction (below) or by monitoring a spectral region beyond the largest expected Doppler shift. (Visible bremsstrahlung is a nearly flat spectral feature in this wavelength band.) The cold Dα line is centered on the rest wavelength of 656.1 nm.

Approaches to removing these "backgrounds" from the spectrum are discussed in some detail in Ref. 9. Some installations use beam modulation to measure the background, some use a toroidally displaced reference view that misses the injected beam, and some attempt to fit the entire spectrum. Beam modulation assumes temporal stationarity of the plasma, while a displaced reference view assumes toroidal symmetry. Neither assumption is perfectly valid. Reference views are available at NSTX (Ref. 4) and, more recently, at DIII-D.[10] A comparison between the two approaches for a condition with relatively low FIDA signal is shown in Fig. 4. The derived spectra are similar but not identical. In the best of circumstances, the systematic uncertainty associated with background subtraction is of O (10%).

The cold Dα line is narrow but very bright. As in a laser scattering measurement, care is required to minimize scattered light in the spectral regions of interest. Temporal variations in background that correlate with fluctuations in the cold Dα intensity have been reported.[11] One expedient is to measure the intensity of the cold Dα feature together with the desired spectrum. Because the cold feature is several orders of magnitude brighter than the FIDA signal, it is usually necessary to filter the cold Dα line to avoid detector saturation.[4,9]

In a DIII-D experiment, Doppler-shifted light from a distant neutral beam reflected off a metallic surface and contaminated the measurements (Fig. 17 of Ref. 6). In general, the line-of-sight for a FIDA measurement should terminate in a blackened surface.

On ASDEX-U, the spectra have fewer contaminating impurity lines when the tokamak gas valve is distant toroidally from the FIDA line-of-sight[12] but this effect is not observed on DIII-D.

In general, three sources of error can contribute to the uncertainty of a measurement: photon statistics, readout and dark current noise, and uncertainty in the background subtraction. In most cases, uncertainty in the background subtraction dominates the overall uncertainty.[11] The challenges are exacerbated by instabilities. A primary purpose of a FIDA diagnostic is to study the impact of instabilities on fast-ion confinement but, unfortunately, instabilities expel particles and heat into the plasma edge, which alters the backgrounds. Figure 11 of Ref. 11 shows an example where simplistic application of a background-subtraction algorithm implies unphysical evolution of the fast-ion density but reasonable corrections for the time-evolving background yield a sensible result.

Figure 5 illustrates various ways to measure the FIDA light. To establish feasibility, nearly every facility begins by tuning an existing charge-exchange recombination instrument to one side of the cold Dα line.[3,8,13–15] The first dedicated FIDA instrument[11] measured the spectrum on both

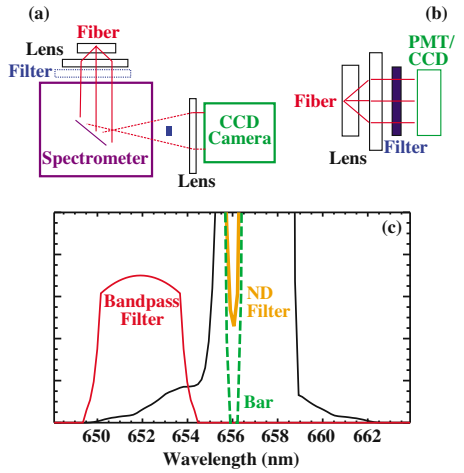

FIG. 5. (Color online) Schematic illustrations of (a) the spectroscopic approach to a FIDA measurement, (b) the bandpass-filtered approach, and (c) the resulting effect on the spectrum. In a spectroscopic measurement, light that is dispersed by a spectrometer is measured with a CCD camera. If the full spectrum is measured, a neutral density filter [solid central curve in (c)] or blocking bar [dashed curve in (c)] placed in the focal plane between the spectrometer and camera attenuates the intensity of the cold Dα line. If only one side of the spectrum is measured, a filter at the entrance to the spectrometer attenuates the cold Dα line. In a f-FIDA or two-dimensional imaging application, a bandpass filter selects the desired spectral band [left curve in (c)] before detection by a photomultiplier or CCD camera.

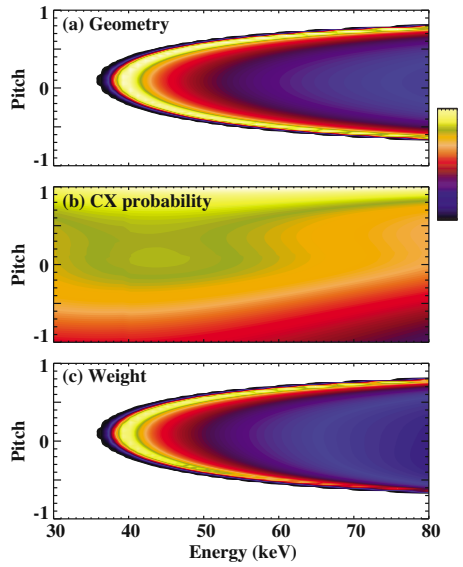

FIG. 6. (Color online) FIDA weight function W vs energy and pitch for a nearly vertical view in DIII-D. The contours are on a linear scale for a blueshifted wavelength corresponding to E_λ=40 keV. (a) Contribution to the weight function associated with measuring a single component of the velocity. (b) Contribution to the weight function associated with variations in neutralization probability. (c) Total weight function W.

sides of the rest wavelength. To avoid saturation of the detector by the cold Dα line, after the light was dispersed by the spectrometer, a solid bar blocked light at 656.1 nm. Subsequently, the bar was replaced by a strip of neutral-density filter (optical density OD2 or OD3) in order to monitor the intensity of the cold line. The NSTX diagnostic uses this approach and employs a high throughput transmission grating spectrometer.[4] If only one side of the line is used, it is convenient to place a bandpass filter at the entrance of the spectrometer and arrange the transmission so the cold line is severely attenuated but still measurable.[9] An alternative approach is to sacrifice spectral resolution for improved temporal or spatial resolution [Fig. 5(b)]. In this approach, the spectrometer is replaced by a filter with a passband of 2–4 nm. For maximal temporal resolution, a photomultiplier replaces the charge-coupled device (CCD) camera, as in the NSTX (Ref. 4) and DIII-D (Ref. 10) "f-FIDA" diagnostics. For improved spatial resolution, light from an imaging fiber-optic bundle passes through a bandpass filter and a two-dimensional image is acquired by a CCD camera.[6]

III. RELATIONSHIP TO THE FAST-ION DISTRIBUTION FUNCTION

The goal of a FIDA measurement is to provide information about the fast-ion distribution function F. In general, the distribution function has a complicated dependence on both velocity-space and configuration-space coordinates. In an axisymmetric tokamak, the distribution function can be expressed as a function of three "constants of motion" but these convenient theoretical coordinates do not correspond to useful laboratory coordinates. A common set of coordinates used by experimentalists is the (E,p,R,z) coordinates used in the TRANSP NUBEAM code,[16] where E is the fast-ion energy, $p=v_\parallel/v$ is the pitch of the fast-ion velocity vector relative to the magnetic field, R is the major radius, and z is vertical position. The challenge addressed in this section is to relate the FIDA spectral intensity versus wavelength to the fast-ion distribution function $F(E,p,R,z)$.

Through the Doppler shift, the FIDA spectrum depends on one component of the fast-ion velocity. In that sense, a FIDA measurement is similar to fast-ion measurements with collective Thomson scattering (CTS), which also depends on one component of the velocity vector. Specialists in CTS have published several papers addressing the relationship between a one-dimensional spectrum and the full distribution function. Egedal and Bindslev[17] rigorously tackle the question: Can you invert a set of CTS measurements to infer the distribution function? They conclude that a unique inversion is impossible but, with multiple CTS viewing angles, plausible reconstructions exist. As the atomic physics of the FIDA process is more complex than the collective scattering process, their conclusion that a unique inversion is impossible certainly applies to FIDA.

A convenient way to understand the relationship between any fast-ion diagnostic and F is to construct a weight function $W(E,p,R,z)$. The measured signal S is the convolution of the weight function with the distribution function

$$S = \int\int\int\int (W * F) dE\ dp\ dR\ dz. \quad (1)$$

Approximate expressions for several common diagnostics are given in Appendix A of Ref. 18. Figure 6(c) shows an example of the velocity-space dependence of the weight function W for a representative vertically viewing FIDA diagnostic. Two factors determine this dependence. The first of these is the geometrical relationship between one velocity component and the variables E and p. Formulas that describe

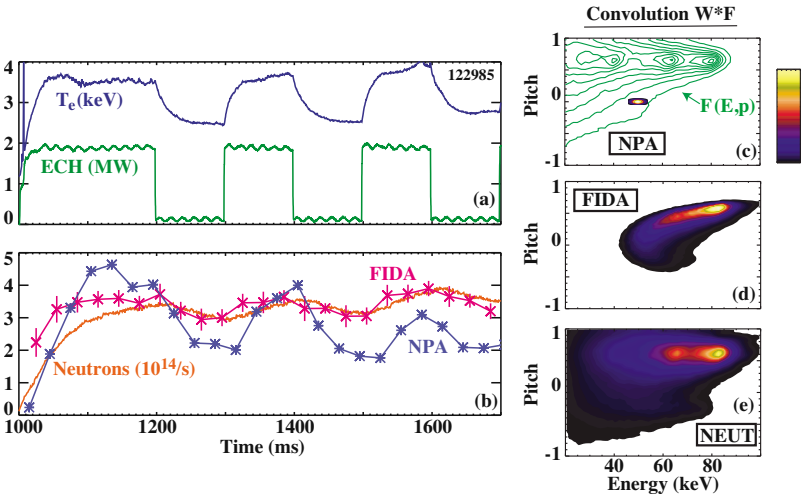

FIG. 7. (Color online) Time evolution of (a) central electron temperature and ECH power and (b) FIDA, NPA, and neutron signals in a DIII-D discharge (Ref. 11) with 2.5 MW of injected beam power from the co-tangential sources. The FIDA signal is integrated over wavelengths corresponding to energy along the line-of-sight of 40–50 keV and is divided by the estimated neutral density at the position of the measurement. The NPA signal is from active charge exchange at the same location as the FIDA channel ($R \cong 196$ cm) and is corrected for changes in neutral density and for attenuation of the escaping neutrals. (c) Contours of the fast-ion distribution function computed by the TRANSP NUBEAM code for this condition. The NPA measures a localized region in velocity space. Product of the weight function W and the distribution function F for (d) the FIDA measurement and (e) the beam-plasma neutron measurement. (c)–(e) adapted and reprinted with permission from W. W. Heidbrink *et al.*, Plasma Phys. Controlled Fusion **49**, 1457 (2007). Copyright © 2007, IOP Publishing Ltd.

this relationship appear in Refs. 6 and 11. Figure 6(a) illustrates this dependence for a view that is nearly perpendicular to the field. The minimum energy that can produce a particular Doppler shift occurs when the fast ion travels directly toward (or away from) the collecting lens; in Fig. 6, this minimum energy is $E_\lambda = 40$ keV. Below this minimum energy, the weight function is zero. Any parallel component of the velocity only increases the energy, which is why the minimum energy is larger for larger values of $|p|$ in Fig. 6(a). Similarly, a fast ion with a different value of gyrophase can also produce a Doppler-shifted photon but only if it has higher energy; this is why the weight function is positive for values of E above the minimum values.

Another important contribution to the weight function is the neutralization probability. Recall that the charge-exchange cross sections are strong functions of energy [Fig. 1(b)]. The relevant quantity is the relative velocity between the fast ion and the neutral, $v_{\rm rel} = |\vec{v}_f - \vec{v}_n|$. The cross sections peak for relatively low values of $v_{\rm rel}$, so the probability of a charge-exchange reaction is increased when the fast ion and the neutral are traveling in similar directions. For the case illustrated in Fig. 6(b), the injected neutral beam travels in the direction of positive pitch p, so the weight function is skewed toward positive values of pitch. There is also an energy dependence to the neutralization probability that reflects the underlying dependence on the cross sections. The velocity-space dependence of this factor would be stronger but two factors reduce the sensitivity: excitations from different energy levels have different cross sections [Fig. 1(b)] and the various neutral species (full, half, third, and halo) have different velocities.

The weight function concept is quite useful in the interpretation of experiments. Figure 7 shows an example from Ref. 11. In this DIII-D experiment, modulated electron cyclotron heating (ECH) modulates the electron temperature T_e in order to study the effect on the neutron, FIDA, and neutral-particle analyzer (NPA) signals. The FIDA and NPA signals are from nearly identical spatial regions in the plasma core. Initially, since both processes rely on active charge-exchange reactions, we expected the FIDA signal to closely resemble the NPA signal but, to our surprise, the FIDA signal more closely resembles the neutron signal (which is predominately from beam-plasma reactions for this condition). Consideration of the weight functions explains this result. The NPA diagnostic measures a localized region in velocity space, so it is very sensitive to variations in the pitch-angle distribution caused by changes in T_e. In contrast, for this experimental arrangement, the neutron and FIDA diagnostics are both sensitive to the bulk of the fast-ion distribution. The signals do increase when T_e increases but the changes are more modest than for the NPA signal. Another example of the utility of the weight-function concept appears in Figs. 14 and 16 of Ref. 6. In this case, a tangentially viewing FIDA diagnostic is only sensitive to the fast-ion population that is circulating toroidally opposite to the plasma current, the so-called counterpassing fast-ion population. When the beam that injects countergoing ions is replaced by a beam that injects in the opposite direction, the tangential-FIDA signal decays rapidly but the neutron and vertical-FIDA signals are barely affected because the latter two diagnostics are sensitive to fast ions throughout velocity space.

Approximate weight functions are convenient for qualitative interpretation of experimental trends but, unfortunately, the actual weight function varies with plasma parameters. In principle, one could compute the weight function for

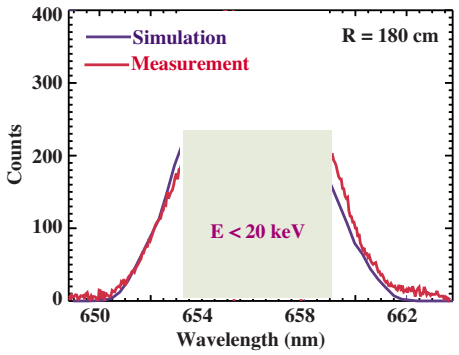

FIG. 8. (Color online) Comparison of the measured FIDA spectrum with the predicted spectrum in a MHD-quiescent DIII-D plasma. For small Doppler shifts ($E_\lambda < 20$ keV), uncertainties in the background subtraction are large. Reprinted with permission from Y. Luo *et al.*, Phys. Plasmas **14**, 112503 (2007). Copyright © 2007, American Institute of Physics.

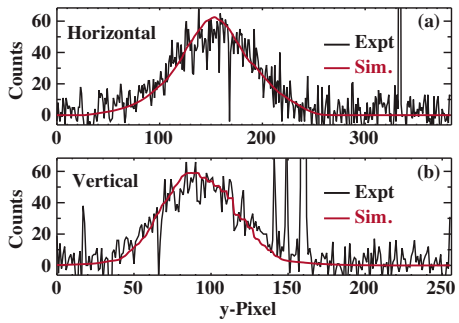

FIG. 9. (Color online) Comparison of DIII-D FIDA imaging data with the predicted profile for (a) horizontal and (b) vertical lines through the maximum of the measured image. Adapted and reprinted with permission from M. A. Van Zeeland *et al.*, Plasma Phys. Controlled Fusion **51**, 055001 (2009). Copyright © 2009, IOP Publishing Ltd.

a particular experimental condition, then multiply W by various model distribution functions F and find which F gives the best agreement with experiment. This approach to inferring the distribution function is used with CTS data;[19] a similar procedure should work with FIDA data.

To date, quantitative comparisons with theory have relied on forward modeling using a weighted Monte Carlo code called FIDASIM. Since a detailed description of this code was recently submitted for publication,[20] only a brief summary is given here. (A description of an initial version of the code also appears in Appendix A of Ref. 3.) The code calculates the neutral populations (including excitation levels) from plasma and neutral beam parameters. A theoretical fast-ion distribution function from, for example, the TRANSP NUBEAM module,[16] is input to the code. Armed with this information, the code computes the neutralization probability, solves the collisional-radiative equations to predict the Balmer-α emission, and computes the spectra (including Stark splitting). For comparison, the code also computes the Dα light from injected and halo neutrals.

The first detailed quantitative comparison of the predicted FIDA spectrum with experiment was reported in Ref. 21. In magnetohydrodynamics (MHD)-quiescent DIII-D plasmas, code predictions based on the fast-ion distribution function predicted by NUBEAM have the same spectral shape as experiment and the intensity of the FIDA signal agrees to within 25% (Fig. 8). This study also explored numerous parametric dependencies and found that the FIDA signal varies as expected with injection energy, injection angle, viewing angle, beam power, electron temperature, and electron density.[21] A later DIII-D experiment[22] also found agreement to within ~25% between the spectral shape, radial profile, and absolute intensity for quiet plasmas with ion temperatures below ~3 keV.

The most detailed study of the FIDA profile shape was performed with a bandpass filter and imaging CCD camera on DIII-D.[6] As shown in Fig. 9, both the vertical and the horizontal profile shapes agree well with code predictions.

Another check on the interpretation of the FIDA signal is to compare the relative magnitudes of the FIDA, injected-neutral, and halo light. In a recent ASDEX-U comparison,[14] the agreement with code predictions is good.

Although acceptable agreement with TRANSP NUBEAM predictions is observed in MHD-quiescent plasmas in conventional tokamaks, a similar study on the NSTX spherical tokamak found discrepancies between theory and experiment. In particular, owing to the large fast-ion gyroradius and large poloidal field in a spherical tokamak, theory predicts asymmetries between the redshifted and blueshifted spectra that have not yet been observed. The source of these discrepancies is currently under investigation.

IV. APPLICATIONS

There are three basic types of FIDA studies (Fig. 10). One type of measurement is to search for changes in spectral shape. For example, during combined neutral beam injection and ion cyclotron heating, fast ions are accelerated above the injection energy, which appears in the FIDA data as a distortion of the spectrum at large Doppler shift [Fig. 10(a)]. This type of measurement is arguably the easiest. Since the measurement is a relative one, uncertainties in absolute intensity are irrelevant. If the heating is steady, the data are accumulated for 100 ms or more to obtain good photon statistics at large Doppler shift.

Another common type of relative measurement is to

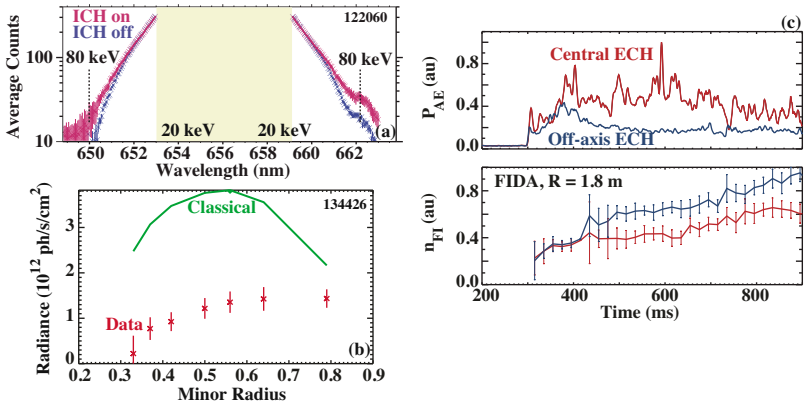

FIG. 10. (Color online) Three types of physics studies. (a) Change in FIDA spectra as a parameter is changed. In this example, fast ions are accelerated when ion cyclotron heating is applied. Adapted and reprinted with permission from W. W. Heidbrink *et al.*, Plasma Phys. Controlled Fusion **49**, 1457 (2007). Copyright © 2007, IOP Publishing Ltd. (b) Comparison of the spatial FIDA profile with the profile predicted by theory. In this example, the measured profile differs dramatically from classical expectations due to fast-ion transport by drift waves. Adapted and reprinted with permission from W. W. Heidbrink *et al.*, Plasma Phys. Controlled Fusion **51**, 125001 (2009). Copyright © 2009, IOP Publishing Ltd. (c) Change in the time evolution of the FIDA signal as plasma parameters change. In this example, application of ECH at different locations modifies the amplitude of Alfvén eigenmode activity, which alters the fast-ion transport. Adapted and reprinted with permission from M. A. Van Zeeland *et al.*, Plasma Phys. Controlled Fusion **50**, 035009 (2008). Copyright © 2008, IOP Publishing Ltd.

measure the time evolution of the signal. In this application, the data are usually integrated over a spectral band. To obtain a signal that is proportional to the fast-ion density in the detected portion of velocity space, the signal is often divided by an estimate of the injected neutral density. For example, in Fig. 10(c) this "FIDA density" decreases when Alfvén eigenmode activity is strong and increases when the activity is partially suppressed. The main technical challenge for this type of measurement is ensuring that changes in background do not obscure the true FIDA evolution. With a bandpass-filtered "f-FIDA" system, ~50 kHz fluctuations in signal have been measured in both NSTX during Alfvén eigenmode activity[23] and in DIII-D plasmas with large neoclassical tearing modes.[10] For the fastest measurements, photon statistics become the limiting factor.

The third type of measurement is a measurement of the FIDA profile after integration over a portion of the spectrum. Initially, several publications relied on relative changes in profile as the discharge evolved[18,21,24] but, in recent years, absolute comparisons of the intensity profile with theory have become common. Figure 10(b) shows an example of a highly discrepant case measured in a high-temperature DIII-D plasma. This type of study is the most challenging, as calibration and background-subtraction uncertainties influence the measurement, while uncertainties in plasma parameters cause uncertainty in the theoretical prediction.

Two detailed comparisons with the classical predictions of the TRANSP NUBEAM code[21,25] were summarized in the previous section. In another experiment, a substantial off-axis fast-ion population was confirmed with FIDA imaging in a study of neutral-beam current drive on DIII-D.[26]

In an early application of FIDA, redistribution of the fast ions was measured in a high-beta DIII-D discharge, confirming modeling that required anomalous fast-ion diffusion.[27] A later DIII-D study measured spectra and profiles that deviate from classical predictions.[22,28] These discharges did not have appreciable MHD activity. The deviations occur in high-temperature plasmas, where fast-ion transport by drift waves is expected.

On DIII-D, strong flattening of the fast-ion profile is measured during Alfvén activity that is driven by the fast-ion population.[24,30] The application of electron cyclotron heating can suppress some of the Alfvén modes and improve fast-ion confinement.[25,29] The changes in FIDA signal correlate with anomalies in plasma rotation.[30,31] Theoretical simulations have successfully accounted for aspects of the FIDA observations.[32–34] A study of a different Alfvén instability, the beta-induced Alfvén-acoustic mode, also found a correlation between mode activity and increased fast-ion transport.[35]

The effect of Alfvén instabilities on FIDA signals has also been studied on NSTX.[23] Sudden drops in signal on a 0.1 ms time scale are observed at "avalanche" events where many Alfvén modes interact.

Although low-frequency MHD modes affect FIDA signals, few results have been published yet. One study on NSTX explored the correlation between FIDA profiles and resistive wall mode stability.[36]

Spectral and profile measurements of rf acceleration of fast ions have been obtained on both DIII-D (Ref. 18) and NSTX.[37,38] A recent theoretical study[39] tries to explain the FIDA data.

FIDA diagnostics are now implemented at six facilities worldwide. At TEXTOR, a tangential view is sensitive to the cocirculating beam ions.[8] At ASDEX-U, changes in profile during off- and on-axes neutral beam injection have been detected.[14] At MAST, a peaked profile is observed during beam injection.[15] On the Large Helical Device, the measured light is produced by hydrogen fast ions[13] rather than deuterium ones but the measurement principle is the same. (A hydrogen fast-ion spectrum has also been measured during hydrogen beam injection on DIII-D.) On DIII-D, new views with a large tangential velocity component have been installed;[9,10] in combination with the existing vertical views, this provides more information about the portion of velocity space that is affected by instabilities. Recent data show that the fractional reduction in FIDA signal at sawtooth instabilities is larger on the tangential signals than on the vertical signals. A new tangentially viewing installation is planned for NSTX.[40]

FIDA is a powerful diagnostic on existing machines. The spectra provide information on one velocity coordinate, the spatial resolution can be a few centimeters in the transverse direction, the temporal resolution can be submillisecond, and calibrated measurements of the radiance permit absolute comparisons with theory. This wealth of information, coupled with the relative simplicity and affordability of visible spectroscopy, make FIDA a preferred diagnostic for machines with positive neutral-beam injection and densities below $n_e \lesssim 6 \times 10^{13}$ cm^{-3}.

Application in ITER or beyond is less promising. One difficulty is that the charge-exchange cross sections peak at relatively low energy [Fig. 1(b)]. This implies that the fast ions that react with an injected beam must have a velocity close to the beam velocity so that the relative velocity is small. Nevertheless, useful information about the fast-ion distribution can still be obtained; see Fig. 12 of Ref. 3. The greater challenge is signal-to-noise. Since the FIDA signal is proportional to the product of fast-ion and injected-neutral density, FIDA works best in low-density plasmas where the fast-ion density is high and the neutral-beam penetration is deep. Moreover, visible bremsstrahlung increases as n_e^2, so this background will be much larger in ITER than in DIII-D. Unless the accuracy of background subtraction significantly exceeds current values, the FIDA feature will be obscured by uncertainties in the background.

ACKNOWLEDGMENTS

This work was funded in part by the U.S. Department of Energy under Grant Nos. SC-G903402, DE-FC02-04ER54698, DE-AC02-09CH11466, and DE-FG02-06ER54867. The instruments discussed here are due to the hard work of K. Burrell, Y. Luo, D. Kaplan, D. Taussig, C. Muscatello, J. Yu, M. Van Zeeland, R. Bell, R. Feder, and M. Podestà. Additional FIDA collaborators include E. Ruskov, D. Liu, B. Geiger, M. García-Muñoz, and Y. Zhu. The data in Fig. 4 were acquired by M. Podestà. None of the measure-

ments would be possible without the dedicated support of the DIII-D and NSTX Teams.

[1] M. G. von Hellermann, W. G. F. Core, J. Frieling, L. D. Horton, R. W. T. Konig, and H. P. Summers, Plasma Phys. Controlled Fusion **35**, 799 (1993).
[2] G. R. McKee, R. Fonck, B. Sratton, R. Bell, R. Budny, C. Bush, B. Grek, D. Johnson, H. Park, A. Ramsey, E. Synakowski, and G. Taylor, Phys. Rev. Lett. **75**, 649 (1995).
[3] W. W. Heidbrink, K. H. Burrell, Y. Luo, N. A. Pablant, and E. Ruskov, Plasma Phys. Controlled Fusion **46**, 1855 (2004).
[4] M. Podestà, W. W. Heidbrink, R. E. Bell, and R. Feder, Rev. Sci. Instrum. **79**, 10E521 (2008).
[5] R. C. Isler, Plasma Phys. Controlled Fusion **36**, 171 (1994).
[6] M. A. Van Zeeland, W. W. Heidbrink, and J. Yu, Plasma Phys. Controlled Fusion **51**, 055001 (2009).
[7] R. J. Fonck, D. S. Darrow, and K. P. Jaehnig, Phys. Rev. A **29**, 3288 (1984).
[8] E. Delabie, R. J. Jaspers, M. G. Von Hellermann, S. K. Nielsen, and O. Marchuk, Rev. Sci. Instrum. **79**, 10E522 (2008).
[9] W. W. Heidbrink, Y. Luo, C. M. Muscatello, C. Y. Zhu, and K. H. Burrell, Rev. Sci. Instrum. **79**, 10E520 (2008).
[10] C. M. Muscatello, W. W. Heidbrink, D. Taussig, and K. H. Burrell, Rev. Sci. Instrum. **81**, 10D316 (2010).
[11] Y. Luo, W. W. Heidbrink, K. H. Burrell, D. H. Kaplan, and P. Gohil, Rev. Sci. Instrum. **78**, 033505 (2007).
[12] M. García-Muñoz, private communication (2010).
[13] M. Osakabe, S. Murakami, M. Yoshinuma, K. Ida, A. Whiteford, M. Goto, D. Kato, T. Kato, K. Nagaoka, T. Tokuzawa, Y. Takeiri, and O. Kaneko, Rev. Sci. Instrum. **79**, 10E519 (2008).
[14] B. Geiger, M. Garcia-Munoz, W. W. Heidbrink, G. Tardini, and R. McDermott, "Fast ion D-alpha measurements at ASDEX Upgrade," Plasma Phys. Controlled Fusion (unpublished).
[15] C. Michael (private communication).
[16] A. Pankin, D. McCune, R. Andre, G. Bateman, and A. Kritz, Comput. Phys. Commun. **159**, 157 (2004).
[17] J. Egedal and H. Bindslev, Phys. Plasmas **11**, 2191 (2004).
[18] W. W. Heidbrink, Y. Luo, K. H. Burrell, R. W. Harvey, R. I. Pinsker, and E. Ruskov, Plasma Phys. Controlled Fusion **49**, 1457 (2007).
[19] M. Salewski, F. Meo, M. Stejner, O. Asunta, H. Bindslev, V. Furtula, S. B. Korsholm, T. Kurki-Suonio, F. Leipold, F. Leuterer, P. K. Michelsen, D. Moseev, S. K. Nielsen, J. Stober, G. Tardini, D. Wagner, P. Woskov, and ASDEX Upgrade Team, Nucl. Fusion **50**, 035012 (2010).
[20] W. W. Heidbrink, D. Liu, Y. Luo, E. Ruskov, and B. Geiger, "A code that simulates fast-ion D-alpha and neutral particle measurements," Comm. Comp. Phys. (submitted).
[21] Y. Luo, W. W. Heidbrink, E. Ruskov, K. H. Burrell, and W. M. Solomon, Phys. Plasmas **14**, 112503 (2007).
[22] W. W. Heidbrink, M. Murakami, J. M. Park, C. C. Petty, M. A. Van Zeeland, J. H. Yu, and G. R. McKee, Plasma Phys. Controlled Fusion **51**, 125001 (2009).
[23] M. Podestà, W. W. Heidbrink, D. Liu, E. Ruskov, R. E. Bell, D. S. Darrow, E. D. Fredrickson, N. N. Gorelenkov, G. J. Kramer, B. P. LeBlanc, S. S. Medley, A. L. Roquemore, N. A. Crocker, S. Kubota, and H. Yuh, Phys. Plasmas **16**, 056104 (2009).
[24] W. W. Heidbrink, N. N. Gorelenkov, Y. Luo, M. A. Van Zeeland, R. B. White, M. E. Austin, K. H. Burrell, G. J. Kramer, M. A. Makowski, G. R. McKee, and R. Nazikian, Phys. Rev. Lett. **99**, 245002 (2007).
[25] M. A. Van Zeeland, W. W. Heidbrink, R. Nazikian, E. Austin, C. Z. Cheng, M. S. Chu, N. N. Gorelenkov, C. T. Holcomb, A. W. Hyatt, G. J. Kramer, J. Lohr, G. R. McKee, C. C. Petty, R. Prater, W. M. Solomon, and D. A. Spong, Nucl. Fusion **49**, 065003 (2009).
[26] J. M. Park, M. Murakami, C. C. Petty, W. W. Heidbrink, T. H. Osborne, C. T. Holcomb, M. A. Van Zeeland, R. Prater, T. C. Luce, M. R. Wade, M. E. Austin, N. H. Brooks, R. V. Budny, C. D. Challis, J. C. DeBoo, J. S. deGrassie, J. R. Ferron, P. Gohil, J. Hobirk, E. M. Hollmann, R. M. Hong, A. W. Hyatt, J. Lohr, M. J. Lanctot, M. A. Makowski, D. C. McCune, P. A. Politzer, H. E. St. John, T. Suzuki, W. P. West, E. A. Unterberg, and J. H. Yu, Phys. Plasmas **16**, 092508 (2009).
[27] M. Murakami, M. R. Wade, C. M. Greenfield, T. C. Luce, J. R. Ferron, H. E. St. John, J. C. DeBoo, W. W. Heidbrink, Y. Luo, M. A. Makowski, T. H. Osborne, C. C. Petty, P. A. Politzer, S. L. Allen, M. E. Austin, K. H. Burrell, T. A. Casper, E. J. Doyle, A. M. Garofalo, P. Gohil, I. A. Gorelov, R. J. Groebner, A. W. Hyatt, R. J. Jayakumar, K. Kajiwara, C. E. Kessel, J. E. Kinsey, R. J. La Haye, L. L. Lao, A. W. Leonard, J. Lohr, T. W. Petrie, R. I. Pinsker, R. Prater, T. L. Rhodes, A. C. C. Sips, G. M. Staebler, T. S. Taylor, M. A. Vanzeeland, G. Wang, W. P. West, L. Zeng, and DIII-D Team, Phys. Plasmas **13**, 056106 (2006).
[28] W. W. Heidbrink, M. Murakami, J. M. Park, C. C. Petty, and M. A. Van Zeeland, Phys. Rev. Lett. **103**, 175001 (2009).
[29] M. A. Van Zeeland, W. W. Heidbrink, R. Nazikian, W. M. Solomon, M. E. Austin, H. L. Berk, N. N. Gorelenkov, C. T. Holcomb, A. W. Hyatt, G. J. Kramer, J. Lohr, M. A. Makowski, G. R. McKee, C. C. Petty, S. E. Sharapov, and T. L. Rhodes, Plasma Phys. Controlled Fusion **50**, 035009 (2008).
[30] W. W. Heidbrink, M. A. Van Zeeland, M. E. Austin, K. H. Burrell, N. N. Gorelenkov, G. J. Kramer, Y. Luo, M. A. Makowski, G. R. McKee, C. Muscatello, R. Nazikian, E. Ruskov, W. M. Solomon, R. B. White, and Y. Zhu, Nucl. Fusion **48**, 084001 (2008).
[31] W. M. Solomon, K. H. Burrell, A. M. Garofalo, A. J. Cole, R. V. Budny, J. S. deGrassie, W. W. Heidbrink, G. L. Jackson, M. J. Lanctot, R. Nazikian, H. Reimerdes, E. J. Strait, M. A. Van Zeeland, and DIII-D Rotation Physics Task Force, Nucl. Fusion **49**, 085005 (2009).
[32] G. Vlad, S. Briguglio, G. Fogaccia, F. Zonca, C. Di Troia, W. W. Heidbrink, M. A. Van Zeeland, A. Bierwage, and X. Wang, Nucl. Fusion **49**, 075024 (2009).
[33] R. B. White, N. Gorelenkov, W. W. Heidbrink, and M. A. Van Zeeland, Plasma Phys. Controlled Fusion **52**, 045012 (2010).
[34] R. B. White, N. Gorelenkov, W. W. Heidbrink, and M. A. Van Zeeland, Phys. Plasmas **17**, 056107 (2010).
[35] N. N. Gorelenkov, M. A. Van Zeeland, H. L. Berk, N. A. Crocker, D. Darrow, E. Fredrickson, G.-Y. Fu, W. W. Heidbrink, J. Menard, and R. Nazikian, Phys. Plasmas **16**, 056107 (2009).
[36] J. W. Berkery, S. A. Sabbagh, R. Betti *et al.*, Phys. Plasmas **17**, 082504 (2010).
[37] D. Liu, W. W. Heidbrink, M. Podestà, R. E. Bell, E. D. Fredrickson, S. S. Medley, R. W. Harvey, and E. Ruskov, Plasma Phys. Controlled Fusion **52**, 025006 (2010).
[38] G. Taylor, R. E. Bell, J. C. Hosea, B. P. LeBlanc, C. K. Phillips, M. Podesta, E. J. Valeo, J. R. Wilson, J-W. Ahn, G. Chen, D. L. Green, E. F. Jaeger, R. Maingi, P. M. Ryan, J. B. Wilgen, W. W. Heidbrink, D. Liu, P. T. Bonoli, T. Brecht, M. Choi, and R. W. Harvey, Phys. Plasmas **17**, 056114 (2010).
[39] M. Choi, D. Green, W. W. Heidbrink, R. Harvey, D. Liu, V. S. Chan, L. A. Berry, F. Jaeger, L. L. Lao, R. I. Pinsker, M. Podesta, D. N. Smithe, J. M. Park, and P. Bonoli, Phys. Plasmas **17**, 056102 (2010).
[40] A. Bortolon, W. W. Heidbrink, and M. Podestà, Rev. Sci. Instrum. **81**, 10D728 (2010).